JOM, Vol. 76, No. 2, 2024
https://doi.org/10.1007/s11837-023-06297-1

Effect of Induced Martensite Content on Microstructure Evolution and Mechanical Properties of Ferritic Stainless Steel

PENGGUANG MA,[1,2] GUOQING ZU ,[1,2,3] DONGYANG LI,[1,2] SHICHENG SUN,[1,2] CHUANG CHEN,[1,2] YAODONG LIU,[1,2] YUPENG LI,[1,2,4] WENBIAO GONG,[1,2] and YING HAN[1,2]

1.—College of Material Science and Engineering, Changchun University of Technology, Changchun 130012, China. 2.—Key Laboratory of Advanced Structural Materials of Ministry of Education, Changchun University of Technology, Changchun 130012, China. 3.—e-mail: guoqingzu@yeah.net. 4.—e-mail: Lyp.ccut@163.com

Due to the ferrite–austenite dual phase at high temperature, the hard martensite phase was introduced into 430 ferritic stainless steel (430 FSS) by rapid cooling. Through thermodynamic calculation and experimental analysis, the influence of martensite on the microstructure, texture, and mechanical properties of 430 FSS during deformation and annealing was studied. The research results show that, after quenching at 800–1150°C, there is a martensite structure along the ferrite grain boundary. The grain size of the ferrite and martensite increases with the increase of the heat-treatment temperature. The hard martensite can effectively break down the ferrite band structure during the cold-rolling deformation process. After high-temperature annealing in the same process, the martensite disappears and the matrix is full ferrite. Among them, the recrystallized grain size of the 1150°C-quenched sheet is larger than that of the 1050°C- and 950°C-quenched strips, showing a stronger γ-fiber recrystallized texture. Also, the finished annealed sheet quenched at 1150°C has a good match of strength and elongation, with a tensile strength of 690.3 MPa and an elongation of 17%.

INTRODUCTION

Stainless steel is not only widely used in military fields such as nuclear energy, national defense, aviation, and ships, but also in civil industries such as transportation, kitchenware, home appliances, and architectural decoration.[1,2] From the perspective of the global stainless steel industry, austenitic stainless steel accounts for the highest proportion, reaching about 75%. However, the use and development of austenitic stainless steel is restricted by the scarcity of global nickel resources and the increasing price.[3,4]

Ferritic stainless steel (FSS) has a history of more than 100 years. On the road of continuously improving its performance, researchers have never stopped exploring and researching. Although its output accounts for 17% of the total output,[5] it has low nickel content, low production cost, low thermal expansion coefficient, and good corrosion resistance.[6–9] Therefore, FSS can be used to replace austenitic stainless steel in some fields.[10] However, its machinability, formability, and mechanical properties still need to be further improved.[11–13]

Researchers have carried out much research work in terms of alloy composition, microstructure control, deformation, and heat-treatment processes to improve the comprehensive properties of FSS.[14–16] Carbon and nitrogen are considered to be one of the important factors for the occurrence of various defects in FSS, such as low plastic formability, high brittle transition temperature, and low corrosion resistance after welding.[17,18] Followed by ultra-low carbon, nitrogen FSS came into being. In addition, the size and uniformity of the structure (i.e., grain size) are important means to control the formability and mechanical properties of FSS. Patra et al.[19] proposed that, according to the Hall–Petch effect,

(Received June 26, 2023; accepted November 20, 2023; published online December 5, 2023)

different grain size aggregations in rolled and annealed sheets lead to different yields under tensile load. At the same time, due to the local difference of the Taylor factor, wrinkling defects occur. By prolonging the rough rolling interval and reducing the final rolling temperature, the cold-rolled annealed structure can have a strong γ-fiber texture. In addition, the phenomenon of grain clusters in the annealed structure can be reduced, other unfavorable orientation textures can be weakened, and the purpose of improving the formability and reducing the defects of wrinkling can be achieved.

When FSS has a high carbon content, austenite transformation occurs at high temperatures. Miyaji et al.[20] paid attention to this point and tried to introduce martensite to improve the wrinkling resistance of FSS thin strips, but it did not attract the attention of most researchers. In recent years, Kimur et al.[21] adjusted the martensite hardness by a tempering process, and carried out fine characterization and in-depth analysis of the subsequent deformation and recrystallization process. Lu et al.[22] introduced quenching and partitioning and quenching and tempering processes into 430 FSS. Although the preparation process was added, the mechanical properties were significantly improved.

In this study, a large amount of 430 FSS was taken as the research object, and the proportion of austenite phase at high temperature was adjusted to obtain different martensite content and shapes. Furthermore, the effects of martensite on the microstructure, texture, and mechanical properties during subsequent deformation and annealing were studied in order to provide a new and easy method for improving the formability and mechanical properties.

EXPERIMENTAL

The 430 FSS used in this experiment was a hot-rolled sheet with a thickness of 2 mm, and the chemical composition is shown in Table I, while the experimental technical route of 430 FSS is shown in Fig. 1. The original 2-mm-thick plate was insulated at different temperatures in a muffle furnace and then quenched in cold water. Next, it was cooled to room temperature and then removed for pickling to remove the surface oxide layer. The pickling was carried out with the ratio of hydrochloric acid and water of 1:1. Finally, it was kept at 950°C for 2 min for recrystallization annealing and then air-cooled to room temperature.

JMatProV7.0 thermodynamic software was used to calculate the equilibrium phase composition of the 430 FSS at different temperatures and the ratio of each phase, and to predict the intermediate phase and phase transition of the material during heating. Combined with heat-treatment experiments and thermodynamic calculations to adjust the content of ferrite and austenite at high temperature, the experimental steel samples were kept at 800–1150°C for 20 min, and then water-cooled to room temperature to obtain different contents and different sizes of the martensite phase. A water-cooled

Table I. Chemical compositions of the studied 430 FSS (wt.%)

Composition	C	Mn	Si	S	P	Cr	N
Content	0.049	0.23	0.35	0.002	0.031	16.24	0.0348

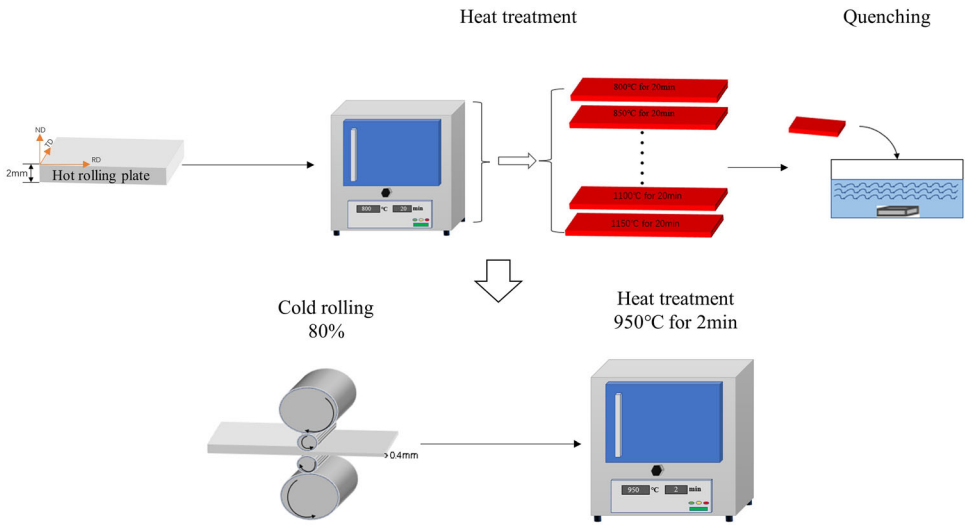

Fig. 1. Heat-treatment and cold-rolling processing route.

430 FSS strip with a representative ferrite–martensite two-phase ratio was selected and rolled to 0.4 mm at room temperature, and the total deformation was 80%. The cold-rolled strip was annealed at 950°C to regain a full ferrite structure through the martensite–austenite–ferrite transformation process.

A Leica Q550IW optical microscope was used to observe the microstructure of the experimental steel at different stages from (RD × TD) sections. The water-cooled and final annealed strips were characterized and analyzed by the EBSD system of a ZEISS ULTRA45 field-emission scanning electron microscope, and the data were post-processed by HKChannel5 software. Tensile experiments were carried out using a DNS200 electronic universal testing machine, the tensile rate was set to 0.5 mm/min, and the fracture properties were characterized and analyzed by scanning electron microscopy. The ASTM E8M[23] sub-sized tensile specimens had a gauge length of 30 mm and a gage width of 6 mm, as shown in Fig. 2.

RESULTS AND DISCUSSION

Thermodynamic Calculation Results

The thermodynamic calculation results of 430 FSS using JMatProV7.0 are shown in Fig. 3. Figure 3a shows the weight fraction of the precipitated phase at different temperatures, and Fig. 4b the comparison of ferrite–austenite at different temperatures. It is not difficult to find that, when the equilibrium temperature was lower than 871°C, the test steel was in the ferrite single-phase region, with only an α-ferrite structure. When the temperature was between 871°C and 1280°C, the experimental steel was in the ferrite–austenite dual-phase region. With the increase of temperature, the weight fraction of austenite first increases and then gradually decreases. When the equilibrium temperature was higher than 1280°C, only a single ferrite structure existed.

In order to more intuitively reflect the three-phase proportion of ferrite–austenite–carbide in 430 FSS at different temperatures, the calculation results of the JMatProV7.0 thermodynamic software are tabulated in Table II. From the calculation results, when the temperature was 800°C and 850°C, the experimental material was the ferrite phase, accounting for about 98.8%. At the same time, there were small amounts of $M_{23}C_6$-type carbide and M_2(C,N)-type compound. When the temperature was 900°C, the proportion of ferrite was 61.73%, the proportion of austenite was 38.12%, and about 0.15% of carbonitride was also present. The carbonitride content decreased with increasing temperature, and there was no carbonitride when the temperature increased to 950°C and above. In general, with the increase of temperature, the content of ferrite phase first decreased and then increased, while, in contrast, the content of austenite phase first increased and then decreased, and the highest austenite content was 44.72% when the temperature was 950°C.

The 430 FSS contains nearly 17 wt.% of Cr, which makes it form a stable single-phase ferrite structure at room temperature. The ultra-low carbon and nitrogen content FSS developed on the basis of 430 FSS has a single-phase ferrite structure even in the high-temperature region. The 430 FSS used in this experiment contained a certain amount of C element, which is an element that expands the austenite phase region, so that the austenite content continues to increase at high temperatures. This provides an important basis for the subsequent

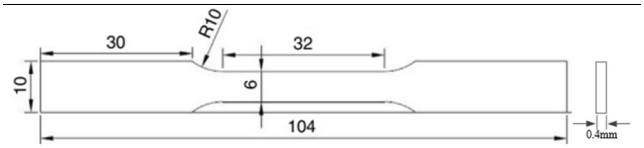

Fig. 2. Dimensions of the specimen used for tensile tests.

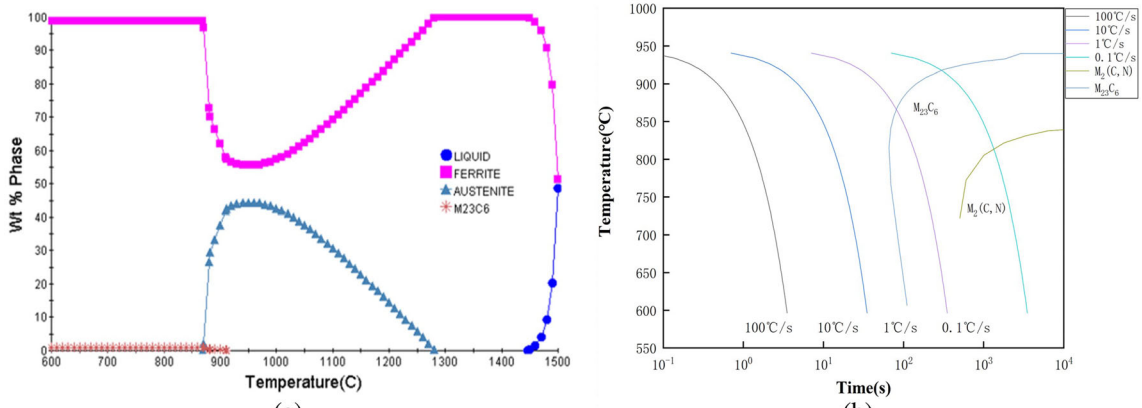

Fig. 3. Weight fraction of the precipitated phase of 430 FSS at different temperatures: (a) weight fraction of precipitates at different temperatures, (b) continuous cooling transformation curve.

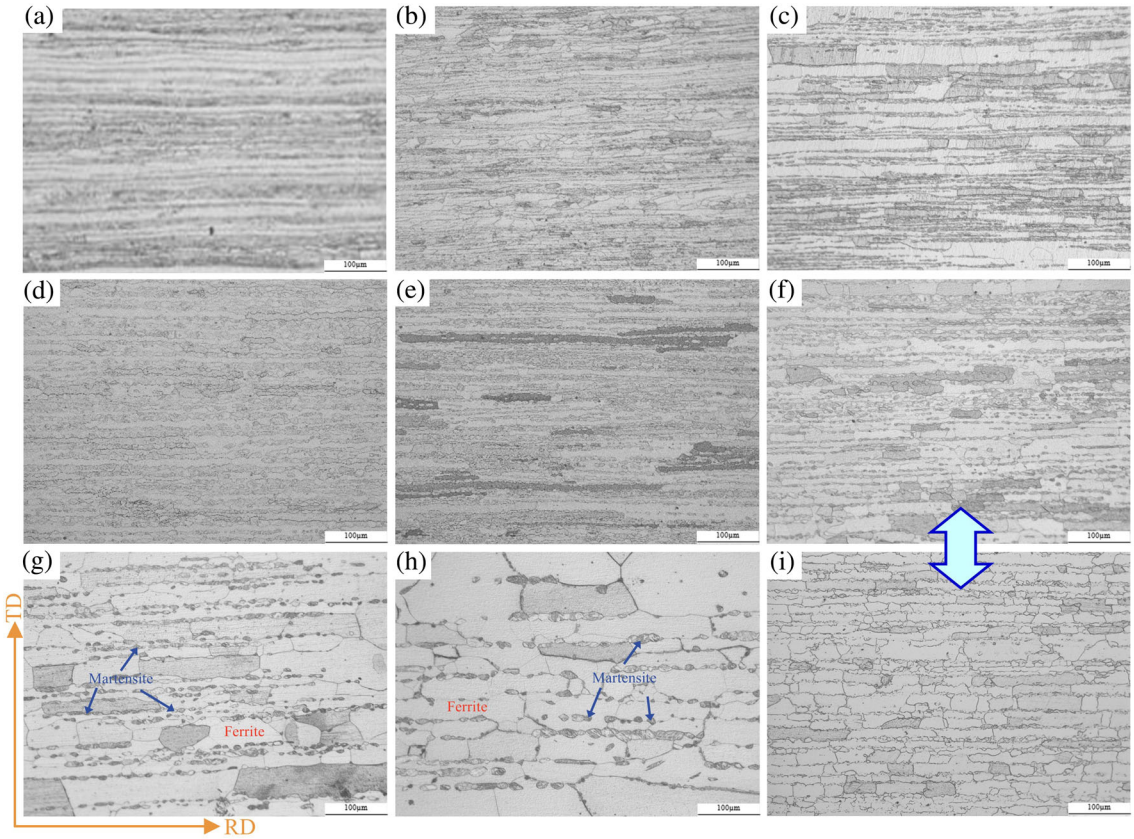

Fig. 4. Microstructure of hot-rolled sheets after different heat treatments photographed using the optical microscope: (a) 800°C, (b) 850°C, (c) 900°C, (d) 950°C, (e) 1000°C, (f) 1050°C water-cooled, (g) 1100°C, (h) 1150°C, (i) 1050°C furnace-cooled.

Table II. The proportion of each component of 430 FSS at different temperatures

Temperature (°C)	Ferrite (wt.%)	Austenite (wt.%)	Carbonitride (wt.%)
800	98.86	–	1.14
850	98.89	–	11.1
900	61.73	38.12	0.15
950	55.28	44.72	–
1000	57.03	42.96	–
1050	62.06	37.93	–
1100	77.06	22.94	–
1150	77.06	22.94	–

regulation of the martensite content in this experiment.

Heat-Treatment Experimental Control Phase Ratio

The water-cooled metallographic structure of the 430 FSS hot-rolled sheet after holding at different annealing temperatures for 20 min are shown in Fig. 4. Between 800°C and 850°C, the 430 FSS is in the single-phase zone of ferrite, and the microstructure after quenching is mainly composed of deformed ferrite grains elongated along the rolling direction. In the heat-treatment range of 900–1150°C, the experimental steel is in the ferrite–austenite dual-phase region, and the martensite phase exists at the ferrite grain boundary after water-cooling. At the same time, with the increase of the heat-treatment temperature, the ferrite crystal grain size gradually becomes larger, and the ferrite layer thickness increases. It can be seen from Fig. 4 that after quenching at 800°C, the ferrite grains retain the elongated state, the boundaries are blurred, and no obvious recrystallized grains and martensite structures are found. After rapid cooling at 900–1150°C, static recrystallization occurs in most areas, and an obvious martensite structure appears at the ferrite grain boundary, with uniform grain size and arrangement, as shown

in Fig. 5. Among them, some strip-like tissues were still retained in the sheet treated at 950°C. With the increase of annealing temperature, the martensite content in the experimental steel first increased and then decreased after quenching. The martensite content in the water-cooled strip after heat preservation at 950°C was the highest, which was consistent with the calculation results of the JMatProV7.0 thermodynamic software. The martensite content was the least in the strip cooled in the furnace after heat preservation at 1050°C, because the austenite at high temperature will be re-transformed into ferrite after heat treatment, as shown in Fig. 4i.

According to the number and size of the martensitic phases after different heat treatments, the quenched strips annealed at 950°C, 1050°C, and 1150°C were selected for subsequent cold-rolling experiments. The microstructures of the three groups of experimental steels before cold rolling are shown in Fig. 5. The ferrite and martensite can be clearly observed, and the size distribution of coarse ferrite grains elongated along the rolling direction at different temperatures is not uniform, showing a trend of increasing with the increase of the annealing temperature of the hot-rolled sheet. Since the heat-treatment temperature is between the ferrite–austenite dual-phase region, the austenite generated during the quenching process correspondingly generates martensite at the ferrite grain boundary. When the heat-treatment temperature was 950°C, the martensite structure was unevenly distributed near the ferrite grain boundary, and the grain size of both was small. When the heat-treatment temperature was 1050°C and 1150°C, the ferrite grains were elongated along the hot rolling direction and the size was coarse. This shows that, as the annealing temperature increases after hot rolling, the ferrite grains grow and the number and size of the recrystallized grains increase. The inverse pole figures (IPF) of the hot-rolled sheet after heat treatment at three selected temperatures are shown in Fig. 5d, e, and f. There are certain numbers of martensitic (α') islands in the martensitic tissue, and the presence of these islands will enhance the hardness of the plate which is proportional to the size of the α' island.[24]

Austenite is generated at the ferrite grain boundaries during the heat treatment of the hot-rolled sheets. As the temperature increases, the ferrite and austenite grains grow gradually.[22] During the rapid cooling process, the dissolved carbon atoms in the austenite have no time to diffuse out of the unit cell, and, when the austenite reaches the martensitic transformation temperature (Ms), the martensitic transformation begins. The parent austenite structure becomes unstable, and then martensite is generated in the austenite grains, as shown in Fig. 5. The increase of martensite will increase the strength of the strip, but reduce the plasticity and toughness, which is usually not conducive to the formability of the strip.[11,25]

Microstructure of Cold-Rolling and Annealing Process

After 80% cold-rolling deformation, the cold-rolled microstructures of the three groups of experimental steels are shown in Fig. 6, from which it can be observed that there is no band-shaped ferrite grains elongated along the rolling direction in the cold-rolled sheet, but a dual-phase alternating structure composed of a large amount of plastically deformed ferrite and deformed martensite is embedded in the ferrite.

The formation of the martensite structure is due to the quenching of the strip, which is dispersed in the ferrite matrix. Since the martensite structure is

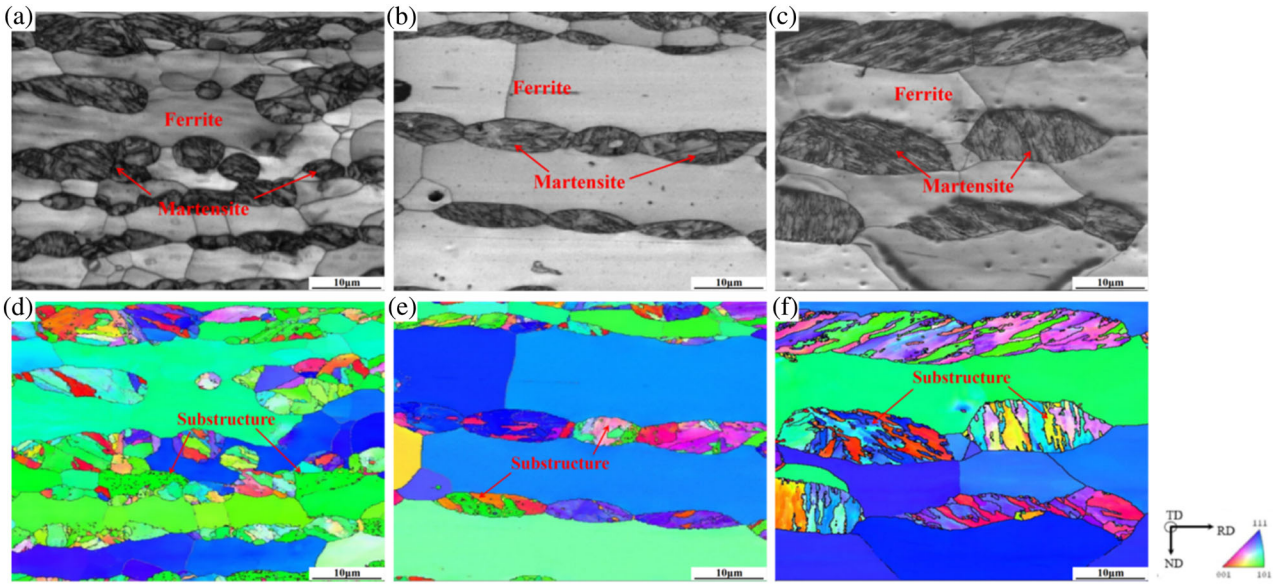

Fig. 5. Microstructure of the quenched plate: (a) and (d) at 950°C, (b) and (e) at 1050°C, (c) and (f) at 1150°C.

harder than the ferrite structure, the two are jointly affected by the rolling force during cold rolling, resulting in different degrees of plastic deformation. Among them, due to the uneven distribution of the martensite structure and the high hardness, the ferrite structure produces a large non-uniform plastic deformation. At the same time, the coarse ferrite grains and the banded ferrite structure during the cold-rolling process are divided by the martensite structure. The grain clusters generated in the FSS hot-rolled sheet are usually difficult to eliminate in the subsequent cold-rolling process, and the introduction of martensite in this experiment can better fragment the ferrite band structure.

A schematic of the martensitic split ferrite matrix during cold-rolling deformation is shown in Fig. 7. Since the martensite structure is introduced at the ferrite grain boundary during the quenching process, during the cold-rolling deformation, the martensite gradually embeds into the ferrite with the increase of the rolling reduction, and then the band-shaped ferrite structure is cut and destroyed to avoid the occurrence of cluster phenomenon.

The metallographic structures of the three groups of strips with different heat-treatment processes after cold-rolling and annealing at 950°C for 2 min are shown in Fig. 8. After annealing, the three groups of cold-rolled sheets all show equiaxed ferrite grains. During the heat preservation process, new ferrite grains nucleated and grew on the deformed matrix, and completely absorbed the deformed matrix after cold rolling, and the martensite disappeared. Figure 9 shows the phase distribution

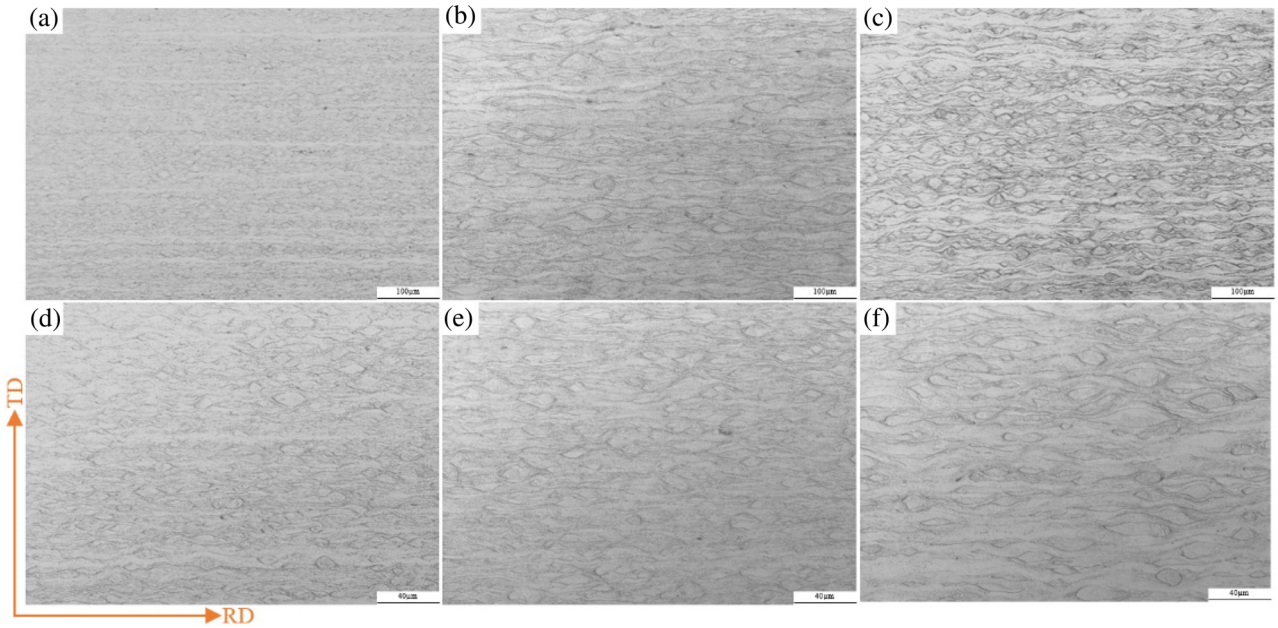

Fig. 6. Metallographic structure of cold-rolled sheet taken with optical microscope: (a), (b), and (c) are the metallographic images of samples taken at 950°C, 1050°C, and 1150°C, respectively, under low magnification; (d), (e), and (f) are metallographic images of samples taken at 950°C, 1050°C, and 1150°C, respectively, at high magnification.

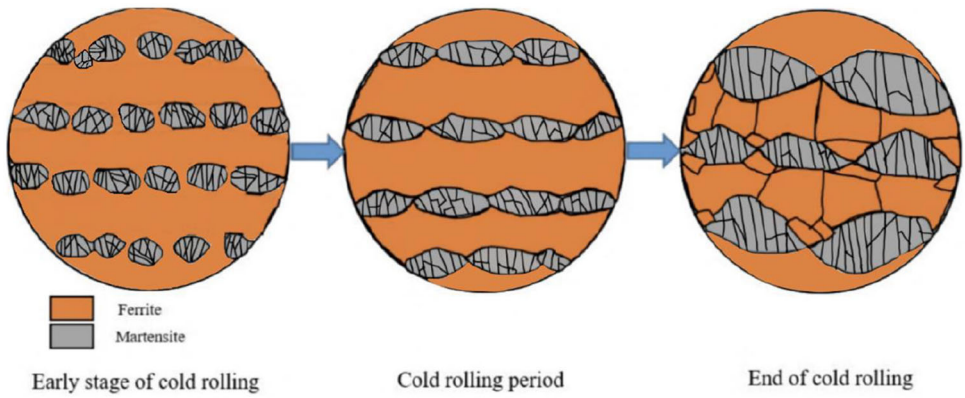

Fig. 7. Schematic of cold-rolling deformation.

diagram of the plate after cold rolling and annealing. After annealing, it is a full ferrite structure. Compared with Fig. 6, it can be found that there is no martensite in the structure after the recrystallization annealing treatment, and that the ferrite grain boundary is clear, and the grain size of the completely recrystallized structure is uniform (Fig. 8). This proves that the martensite structure has been completely transformed into ferrite after cold rolling and annealing. At this time, only ferrite exists in the strip, which has good formability.

However, compared with the structure after cold-rolled annealing, the initial hot-rolled plate is dominated by deformed grains and fiber layers that are elongated in the rolling direction. In addition, dynamic recrystallization of new grains appears in some fiber layers, as shown in Fig. 8. Since the martensite structure is introduced into the hot-rolled sheet by rapid cooling after annealing, the martensite that is unevenly distributed in the ferrite matrix after large plastic deformation of cold rolling will cut and destroy the banded structure and avoid the formation of clusters. During the annealing of the cold-rolled sheets, the unevenly distributed martensite structure provides a site for the nucleation of recrystallized grains. At the same

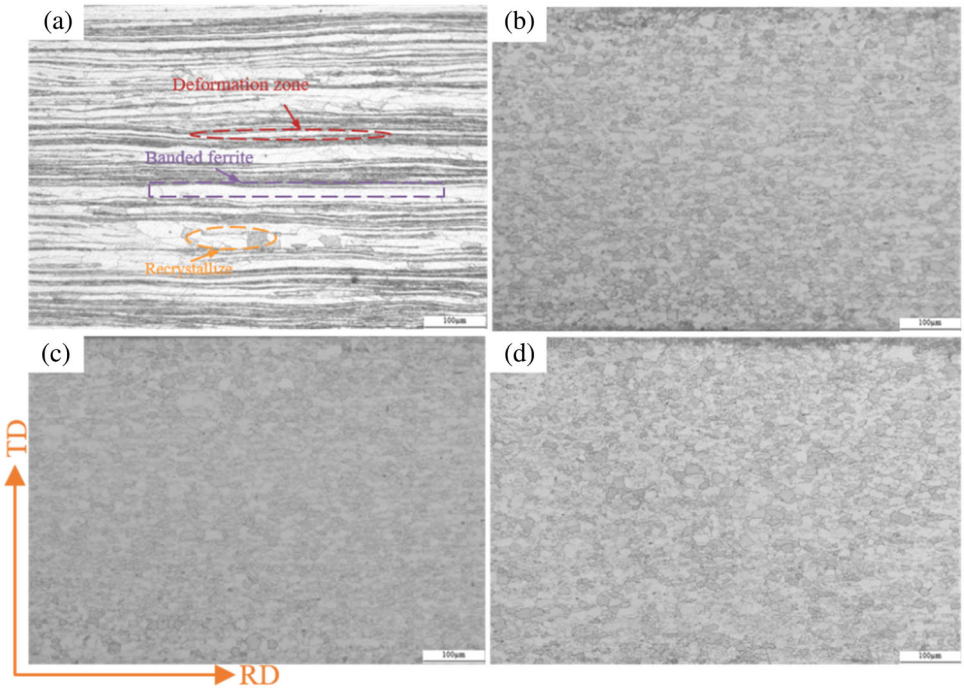

Fig. 8. The metallographic structure of hot-rolled and recrystallized plates was observed with light microscopy: (a) hot-rolled sheet, (b) 950°C, (c) 1050°C, (d) 1150°C.

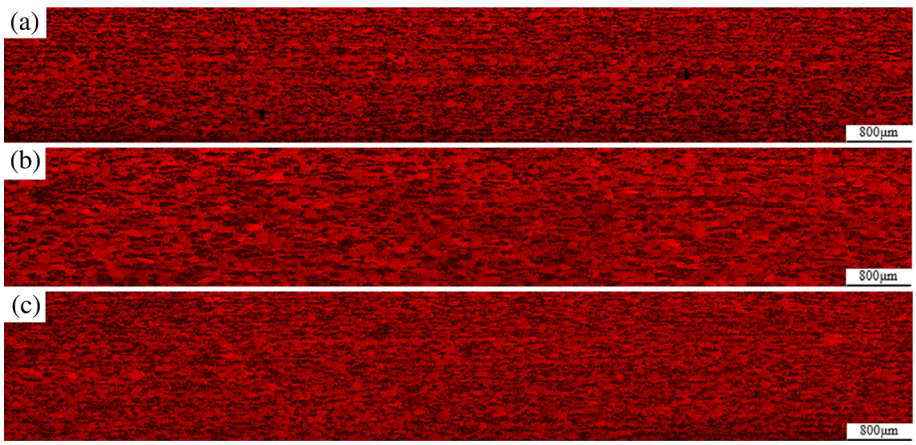

Fig. 9. Phase distribution diagram of the plate after cold rolling and annealing: (a) 950°C, (b) 1050°C, (c) 1150°C.

time, the decomposition of martensite is promoted to obtain ferrite, and the grain size obtained is as uniform as possible to achieve the purpose of improving the formability of stainless steel.[26]

Mechanical Properties of Annealed Sheet

After heat treatment at three selected temperatures, the IPF and orientation distribution function (ODF) diagrams of the cold-rolled sheet annealed at 950°C for 2 min and air-cooled to room temperature are shown in Fig. 10. It can be seen that the three groups of strips are dominated by the γ-fiber recrystallized texture, and that there is a certain amount of α-fiber texture. At the same time, there is no cluster phenomenon or residual martensite structure in the strip. The grain size increases gradually with the increase of the quenching temperature of the initial hot-rolled sheet. The flat, curved grains and a small amount of band-like structure in the cold-rolled and annealed sheet after heat treatment at 950°C are beneficial to improve the strength of the final sheet. The orientation gradient that exists inside the grains is due to the introduction of substructures during rolling deformation, which disappear with increasing temperature. Meanwhile, the γ-fiber recrystallized texture (at $\{111\} < 112 >$) in the strip heat-treated at 1150°C was significantly higher than that in the 950°C-heat-treated strip (at $\{111\} < 561 >$), as shown in Fig. 10d, e, and f. Analysis found that the FSS cold rolling annealing texture is mainly composed of α-fiber ($<110>$ //RD) texture and γ-fiber ($<111>$ //ND) texture.[5] Wright et al.[27] showed that the $\{001\} < 110 >$ orientation is not conducive to the formability of the material, while the $\{111\} < 112 >$ texture is beneficial to improve the formability of the material. Therefore, the hot-rolled annealed strip with strong $\{111\} < 112 >$ texture has better formability. Based on the above reasons, the strength of the strip heat-treated at 950°C increases while the plasticity and toughness decrease, and the strip heat-treated at 1150°C has the second highest strength and the highest elongation, as shown in Fig. 11.

In order to improve the mechanical properties of stainless steel and ensure the stretch formability during the forming process, it is required to have a uniform {111} orientation parallel to the rolling plane and weaken the {100} orientation.[28,29] The {100}-oriented band structure is divided by the martensite introduced after heat treatment during the cold-rolling process, thereby reducing the {100} orientation in the cold-rolled annealed strip.

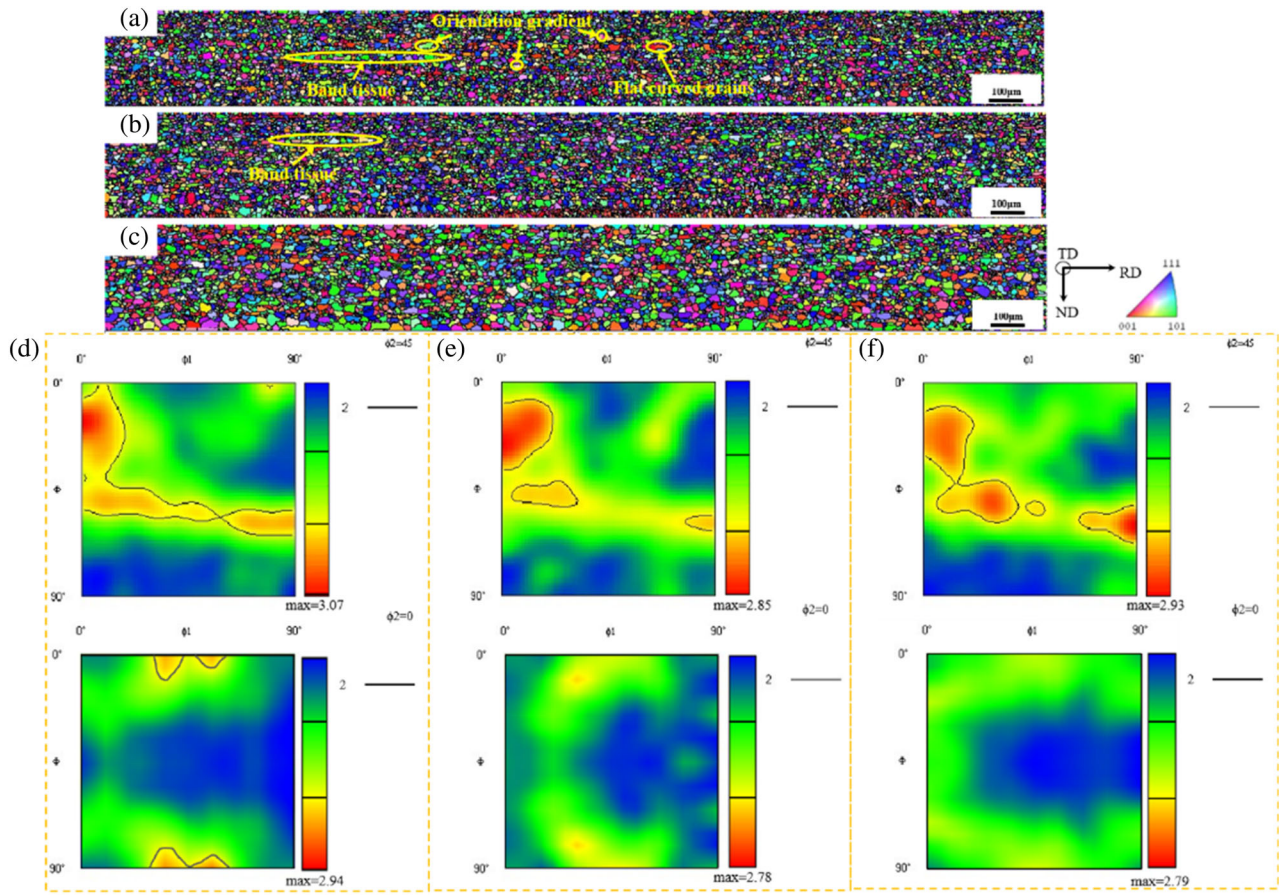

Fig. 10. IPF diagrams and ODF diagrams of cold-rolled annealed sheet: (a), (b), (c) are the IPF diagrams at 950°C, 1050°C, and 1150°C, respectively; (d), (e), and (f) are the ODF diagrams at 950°C, 1050°C, and 1150°C, respectively.

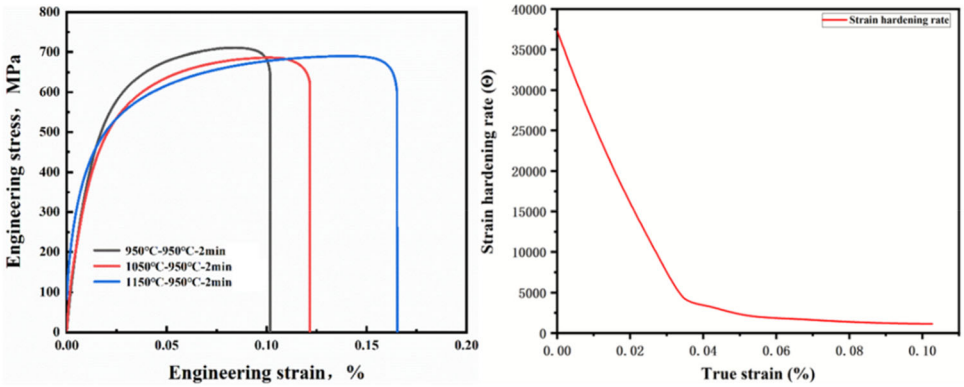

Fig. 11. Stress–strain curve and strain-hardening rate curve of cold-rolled annealed plate: (a) stress–strain curve, (b) strain-hardening curve.

Tensile properties and plastic-forming properties are closely related to the size, number, and texture of recrystallized grains.[30] When it has strong tensile properties and good forming properties, the recrystallization degree of FSS is sufficient and the grain size is a uniform equiaxed grain structure, and the recrystallized texture shows a strong γ-fiber recrystallized texture.

The tensile curves of cold-rolled and annealed strips of 430 FSS after heat treatment at different temperatures are shown in Fig. 11. Compared with the initial hot-rolled plate engineering stress, the stress increased by 30–40%.[11,14,31,32] When the heat treatment temperature was at 950°C, due to the existence of a small amount of strip structure and intragranular orientation gradient in the strip, the tensile strength was better than for the other two groups, reaching 710.4 MPa, and the elongation was the lowest, at 11%. The tensile strength was 687.0 MPa, and the corresponding heat-treatment temperature was 1050°C when the elongation was 12%. At this time, the tensile strength was at the lowest level of the three groups of strips, and the elongation was in the middle. The tensile strength of the strip heat-treated at 1150°C was 690.3 MPa. However, since the average grain size of ferrite in the strip was 9–11 μm, which is at a relatively small level, and has a strong $\{111\} < 112 >$ texture, the elongation performance was the best, reaching 17%. The results show that the corresponding cold-rolled annealed strip after hot-rolling and quenching at 1150°C had better elongation, and that the corresponding cold-rolled and annealed strip had better tensile strength when the heat-treatment temperature was 950°C. It can be seen from Fig. 10d, e, and f that, when the hot-rolled annealing temperature was 1150°C, the γ-fiber texture of the cold-rolled annealed strip was the strongest. The recrystallized texture strength of the γ-fibers is very important to the formability of stainless steel. Therefore, in the recrystallization process of hot-rolled sheets, the α-fiber orientation needs to be reduced, while the enhancement of γ-fiber orientation is relatively beneficial to improve the formability of stainless steel.[33]

The fracture scans of the cold-rolled and annealed strip after three groups of selected temperature heat treatments are shown in Fig. 12. According to the existence of a large number of dimples in the fracture morphology, it can be judged that the three groups of cold-rolled and annealed strips are all plastic fractures. Compared with the fractures of cold-rolled and annealed strips after heat treatment at 950°C, the number of dimples in the fractures of cold-rolled and annealed strips with heat-treatment temperatures of 1050°C and 1150°C increased significantly, the diameters increased significantly, and the dimple depths increased. Among them, the cold-rolled annealed strip with the hot-rolled annealing temperature of 1150°C has the most dimples, the largest dimple diameter, and the deepest dimples due to its completely recrystallized structure and strong γ-fiber texture. Therefore, the plasticity of this group of strips is the best, and the elongation is higher than that of the other two groups, which is consistent with the result of the tensile curves.

CONCLUSION

In this paper, 2-mm-thick hot-rolled stainless steel plates were heat-treated at different temperatures to achieve control of the ferrite–martensite ratio. According to the quantity and size of the martensitic phase, three groups of steel strips heat-treated at different temperatures were selected for subsequent deformation and annealing experiments. The microstructure and final mechanical properties under each process were observed and analyzed, and the following conclusions were drawn:

1. When the hot-rolled strip is quenched after heat treatment, the martensite structure will be precipitated at the ferrite grain boundary. With the increase of temperature, the grain size of both increases, and the martensite content first

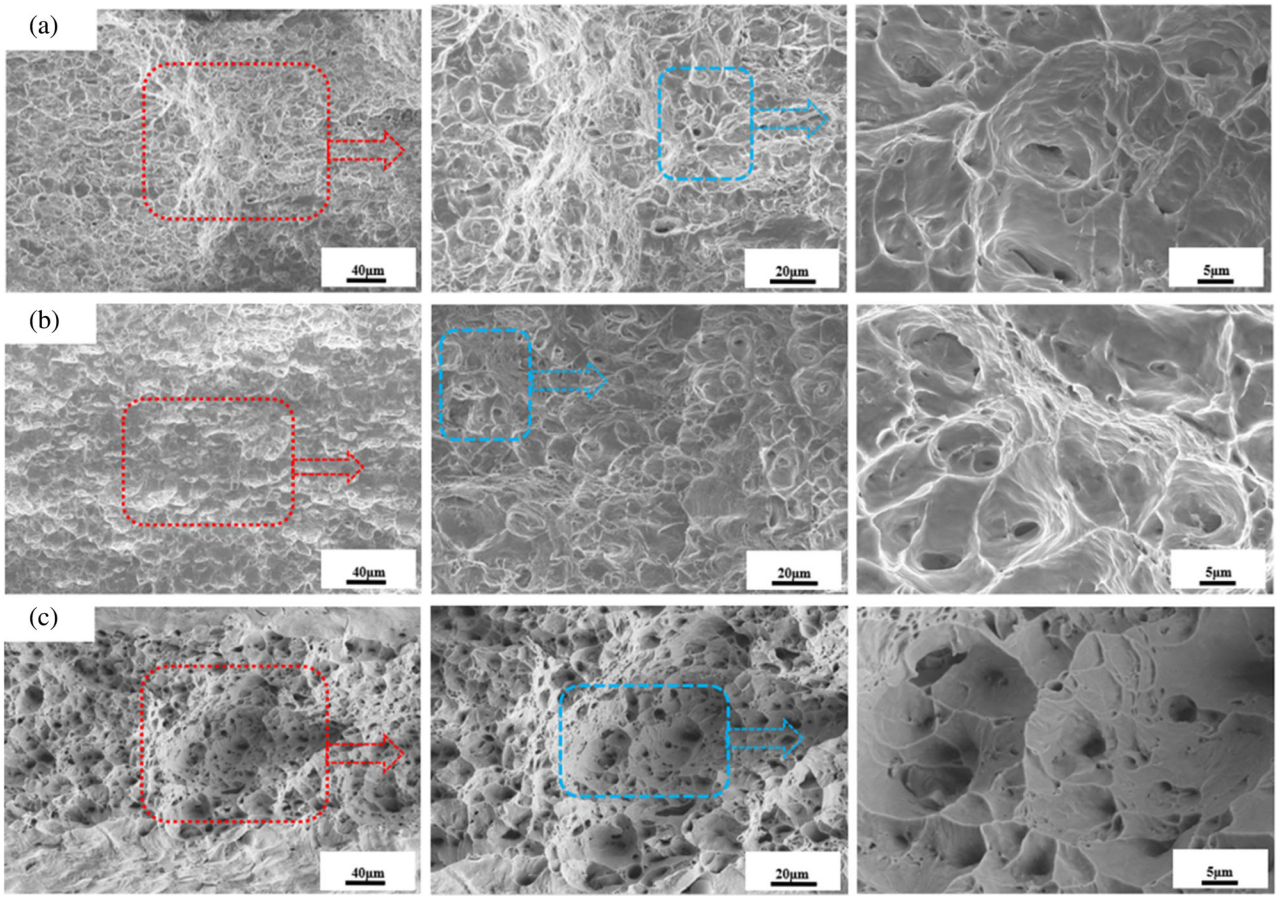

Fig. 12. Fracture morphologies of cold-rolled and annealed sheets after different heat-treatment temperatures: (a) 950°C, (b) 1050°C, (c) 1150°C.

increases and then decreases. The martensite content in the water-cooled strip after heat preservation at 950°C was the highest. In addition, the martensite is more uniform at the ferrite grain boundaries.

2. After 80% cold rolling, there is a dual-phase alternating structure of ferrite and martensite in the strip. In addition, the martensite embedded in the ferrite plays the role of splitting and destroying the banded ferrite, avoiding the occurrence of clustering, which is beneficial to the formability of the strip.
3. After the cold-rolled strips were annealed, they were all completely recrystallized, showing a strong < 111 > //ND texture, which is beneficial to the formability of stainless steel. The hot-rolled annealing temperature of 1150°C showed the strongest γ-fiber recrystallized texture with the highest elongation of 17%.

ACKNOWLEDGEMENTS

The authors acknowledge the National Natural Science Foundation of China (Nos. 52174355, 51701021 and 51974032), the China Postdoctoral Science Foundation funded project (Nos. 2021M693904 and 2022T150074), and the Science and Technology Development Program of Jilin Province (No. 20230201149GX).

CONFLICT OF INTEREST

On behalf of all authors, the corresponding author states that there is no conflict of interest.

REFERENCES

1. C.C. Tasan, M. Diehl, D. Yan, M. Bechtold, F. Roters, L. Schemmann, C. Zheng, N. Peranio, D. Ponge, M. Koyama, K. Tsuzaki, and D. Raabe, *Annu. Rev. Mater. Res.* 45, 391 https://doi.org/10.1146/annurev-matsci-070214-021103 (2015).
2. H.-K. Guo, H.-H. Lu, W.-G. Zhang, L.-X. Meng, and W. Liang, *Mater. Sci. Technol.* 35, 1212 https://doi.org/10.1080/02670836.2019.1618047 (2019).
3. Q.B. Liu, Z.Y. Hu, X.J. Liu, and C.Q. Yang, *Mater. Sci. Forum* 996, 191 https://doi.org/10.4028/www.scientific.net/MSF.996.191 (2020).
4. M. Pan, X. Zhang, P. Chen, X. Su, and R.D.K. Misra, *Mater. Sci. Eng. A.* https://doi.org/10.1016/j.msea.2020.139540 (2020).
5. S. Mehtonen, L.P. Karjalainen, and D.A. Porter, *Mater. Sci. Forum* 762, 705 https://doi.org/10.4028/www.scientific.net/MSF.762.705 (2013).
6. J.-I. Hamada, Y. Matsumoto, F. Fudanoki, and S. Maeda, *ISIJ Int.* 43(12), 1989 (2003).
7. Y. Yu, S. Shironita, K. Souma, and M. Umeda, *Heliyon*. https://doi.org/10.1016/j.heliyon.2018.e00958 (2018).

8. L. Tanure, C.M.D. Alcântara, D.B. Santos, T.R.D. Oliveira, B.M. Gonzalez, and K. Verbeken, *J. Mater. Res. Technol.* 8, 4048 https://doi.org/10.1016/j.jmrt.2019.07.015 (2019).
9. M.E. Korkmaz, *J. Market. Res.* 9, 6322 https://doi.org/10.1016/j.jmrt.2020.03.045 (2020).
10. Y. Bai, T. He, D. Guo, X.-T. Liu, F.-Y. Shao, and Y.-D. Liu, *Acta Metallurgica Sinica (English Letters)* 32, 1362 https://doi.org/10.1007/s40195-019-00895-2 (2019).
11. M. Okayasu and D. Ishida, *Metall. Mater. Trans. A* 50, 1380 https://doi.org/10.1007/s11661-018-5083-4 (2019).
12. R. Iquilio Abarzúa, E. Hernández-Durán, T. Nguyen-Minh, L.A.I. Kestens, J.L. Valín Rivera, and F.M. Castro Cerda, *Steel Res. Int.* https://doi.org/10.1002/srin.202100114 (2021).
13. L. Meng, H. Lu, W. Li, H. Guo, J. Tian, and W. Liang, *Mater. Sci. Eng. A*. https://doi.org/10.1016/j.msea.2021.141191 (2021).
14. X. Ma, J. Zhao, W. Du, X. Zhang, L. Jiang, and Z. Jiang, *J. Market. Res.* 8, 2041 https://doi.org/10.1016/j.jmrt.2018.12.019 (2019).
15. X. Sun, L. Ma, J. Li, M. Zhang, and X. Ma, *Int. J. Adv. Manuf. Technol.* 123(3–4), 1159 https://doi.org/10.21203/rs.3.rs-1716355/v1 (2022).
16. Z. Wang, J. Dirrenberger, P. Lapouge, and S. Dubent, *Mater. Sci. Eng. A*. https://doi.org/10.1016/j.msea.2021.142205 (2022).
17. Y.K.Y. Yazawa and M. Kobayashi, *Kawasaki Steel Technical Report English Edition* (1999), p. 23-29.
18. M.H. Lee, R. Kim, and J.H. Park, *Sci. Rep.* 9, 6369 https://doi.org/10.1038/s41598-019-42879-3 (2019).
19. S. Patra, A. Ghosh, J. Sood, L.K. Singhal, A.S. Podder, and D. Chakrabarti, *Mater. Des.* 106, 336 https://doi.org/10.1016/j.matdes.2016.05.100 (2016).
20. H. Miyaji and S. Watanabe, *J. Japan Inst. Met. Mater.* 39(2), 194 https://doi.org/10.2320/jinstmet1952.39.2_194 (1975).
21. K. Kimura, K. Ushioda, E. Ishimaru, and A. Takahashi, *Mater. Sci. Eng. A* 663, 86 https://doi.org/10.1016/j.msea.2016.03.078 (2016).
22. H.-H. Lu, H.-K. Guo, W.-G. Zhang, and W. Liang, *Mater. Lett.* 240, 275 https://doi.org/10.1016/j.matlet.2019.01.029 (2019).
23. A.I.C.E.-O.M. Testing, *Standard Test Methods for Tension Testing of Metallic Materials* (ASTM International, 2016).
24. S. Basu, B.N. Jaya, A. Patra, S. Ganguly, M. Dutta, A. Hohenwarter, and I. Samajdar, *Metall. Mater. Trans. A* 52, 4018 https://doi.org/10.1007/s11661-021-06361-y (2021).
25. H.-H. Lu, W.-Q. Li, L.-Y. Du, H.-K. Guo, W. Liang, W.-G. Zhang, and Z.-G. Liu, *Mater. Sci. Eng. A* 754, 502 https://doi.org/10.1016/j.msea.2019.03.110 (2019).
26. Y. Shao, C. Liu, T. Yue, Y. Liu, Z. Yan, and H. Li, *Metall. Mater. Trans. B* 49, 1560 https://doi.org/10.1007/s11663-018-1273-0 (2018).
27. R.N. Wright, *Metall. Mater. Trans. B* 3, 83 https://doi.org/10.1007/bf02680588 (1972).
28. C.-Z. Lu, Z. Fang, and J.-Y. Li, *Mater Charact* 135, 257 https://doi.org/10.1016/j.matchar.2017.11.049 (2018).
29. G. Cai, C. Li, D. Wang, and Y. Zhou, *Mater Charact* 141, 169 https://doi.org/10.1016/j.matchar.2018.04.031 (2018).
30. W. Qin, J. Li, Y. Liu, J. Kang, L. Zhu, D. Shu, P. Peng, D. She, D. Meng, and Y. Li, *Mater. Lett.* 254, 116 https://doi.org/10.1016/j.matlet.2019.07.058 (2019).
31. M. Okayasu and T. Shigeoka, *J. Mater. Eng. Perform.* 28, 6771 https://doi.org/10.1007/s11665-019-04426-z (2019).
32. J.D. Zhige Wang, P. Lapouge, and S. Dubent, *Mater. Sci. Eng. A* 831, 142 (2022).
33. A. Després, J.D. Mithieux, and C.W. Sinclair, *Acta Mater.* https://doi.org/10.1016/j.actamat.2021.117226 (2021).